Measurement report: Ambient volatile organic compounds (VOCs) pollution at urban Beijing: characteristics, sources, and implications for pollution control

Lulu Cui[1], Di Wu[1], Shuxiao Wang[1,2*], Qingcheng Xu[1], Ruolan Hu[1], Jiming Hao[1, 2]

[1] *State Key Joint Laboratory of Environment Simulation and Pollution Control, School of Environment, Tsinghua University, Beijing 100084, China*

[2] *State Environmental Protection Key Laboratory of Sources and Control of Air Pollution Complex, Beijing 100084, China*

* Corresponding author. E-mail address: shxwang@tsinghua.edu.cn

Abstract

The increasing ozone (O_3) pollution and high fraction of secondary organic aerosols (SOA) in fine particle mass highlighted the importance of volatile organic compounds (VOCs) in air pollution control. In this work, a campaign of comprehensive field observations was conducted at an urban site in Beijing, from December 2018 to November 2019, to characterize VOCs sources and their contributions to air pollution. The total mixing ratio of the 95 quantified VOCs (TVOC) observed in this study ranged from 5.5–118.7 ppbv with the mean value of 34.9 ppbv. Alkanes, OVOCs and halocarbons were the dominant chemical groups, accounting for 75-81% of the TVOCs across the sampling months. The molar ratios of VOCs to NO_X indicated that O_3 formation was limited by VOCs during the whole sampling period. Positive matrix factorization (PMF) analysis showed that diesel vehicle exhaust, gasoline vehicle exhaust and industrial emissions were the main VOCs sources during both the O_3-polluted and $PM_{2.5}$-polluted months. On the base of O_3 formation impact, VOCs from fuel evaporation and diesel exhaust particularly toluene, xylenes, trans-2-butene, acrolein, methyl methacrylate, vinyl acetate, 1-butene and 1-hexene were the main contributors, illustrating the necessity of conducting emission controls on these pollution sources and species for alleviating O_3 pollution. Instead, VOCs from diesel exhaust and

coal/biomass combustion were found to be the dominant contributors for secondary organic aerosol formation potential (SOAFP), particularly the VOC species of toluene, 1-hexene, xylenes, ethylbenzene and styrene, and top priority should be given to these for the alleviation of haze pollution. This study provides insights for government to formulate effective VOCs control measures for air pollution in Beijing.

Key words: VOCs, OFP, SOAFP, Source appointment

1. Introduction

The ozone (O_3) and fine particulate matter ($PM_{2.5}$) pollution has restricted improvements in air quality in China. Observation data from the Chinese Ministry of Environment and Ecolgy (MEE) network has witnessed an upward trend for O_3 across the country over the period 2013-2019 (Fu et al., 2019; Li et al., 2017; Li et al., 2020; Shen et al., 2019; Fan et al., 2020). Besides, haze pollution occurred in urban sites in recent years were commonly characterized by enhanced formation of secondary organic aerosols (SOA) in fine particles, e.g., the fraction of SOA in organic aerosols reached 58% in Xi'an during winter 2018 and 53% in urban Beijing during winter 2014(Kuang et al., 2020; Li et al., 2017b; Sun et al., 2020; Xu et al., 2019). Volatile organic compounds (VOCs) are key precursors for the formation of O_3 via gas-phase reactions (Odum et al., 1997; Atkinson, 2000; Sato et al., 2010; Huang et al., 2014). In highly polluted urban regions, the O_3 formation was generally VOCs-limited, and it is suggested that VOCs emission control is necessary for effective alleviation of photochemical smog (Liu et al., 2020a,b; Shao et al., 2009; Wang et al., 2020; Xing et al., 2011). Besides, the VOCs compounds including aromatics and biogenic species have significant impact on SOA formation which play an important role in haze formation (Huang et al., 2014; Tong et al., 2021). VOCs emission abatement is therefore imperative for improving air quality in China.

VOCs in ambient air can be emitted by a variety of sources including both anthropogenic and biogenic sources. While biogenic emissions are significantly greater than anthropogenic emissions globally (Doumbia et al., 2021; Sindelarova et al., 2022), anthropogenic emissions play the dominant role in urban and surrounding areas (Warneke et al., 2007; Ahmad et al., 2017; Wu and Xie, 2018). The VOC observations in China showed distinct differences in anthropogenic sources among different regions. For example, solvent use and vehicle exhaust are primary VOCs sources in urban Shanghai and urban Guangzhou, while the primary sources of VOCs

in Wuhan, Zhengzhou and Beijing cities are combustion and vehicle exhaust (Han et al., 2020; Shen et al., 2020; Liu et al., 2020a; Li et al., 2019a). Apart from the diversity of emission sources, different VOCs species exhibited different propensities to form O_3 and SOA. Observation-based studies commonly applied the O_3 formation potential (OFP) and SOA formation potential (SOAFP) scales to quantify the relative effects of specific VOCs and sources on O_3 and SOA formation and to aid in the development of efficient control strategies (Carter and Atkinson, 1989; Chang and Rudy, 1990; Han et al., 2020; Zhang et al., 2017). Although there have been many studies on ambient VOCs in various locations (e.g., urban, rural, and industrial areas), most of these measurements were confined to short periods (a few days or a certain season), and the understanding of temporal variations of concentrations, sources as well as the influence of photochemical reactions of VOCs on annual scale was still limited. Besides, most of the available reports on VOCs analysis based on online analytical techniques include mainly non-methane hydrocarbon compounds, and thus the characteristics of VOCs as well as their relationships with $PM_{2.5}$ and O_3 cannot be fully revealed since OVOC also participate actively in chemical reactions related to secondary formation (Li et al., 2019a; Zhao et al., 2020; Yang et al., 2018; Sinha and Sinha., 2019). Therefore, the long-term and comprehensive monitoring of VOCs are desired.

As the capital and one of the largest megacities in China, Beijing has been suffering from severe O_3 pollution due to rapid economic development and increases in precursor emissions (Wang et al., 2014a; Wang et al, 2017; Li et al., 2019d; Zhao et al., 2020). According to the Report on the State of the Ecology and Environment in Beijing, the average 90th percentile O_3 daily maximum 8 h concentration in Beijing exceeded the national standards, reaching 193, 192, and 191 $\mu g/m^3$ in 2017, 2018, and 2019, respectively. In addition, the number of motor vehicles in Beijing reached 6.365 million at of the end of 2019 (http:// beijing.gov.cn), making Beijing the top city in China in terms of number of motor vehicles. The existing field measurements in Beijing were mostly

conducted before 2016, and the observation in most recent years is quite limited (Li et al., 2015; Li et al., 2019c; Liu et al., 2020a; Yang et al., 2018). In this work, a campaign of comprehensive field observations was conducted at an urban site in Beijing during December 2018 and November 2019 for the analysis of VOCs. Several O_3 and $PM_{2.5}$ pollution events were captured during the sampling period. The characteristics and the contribution of specific species and sources of VOCs on O_3 and SOA formation, with a focus on photochemical and haze pollution periods, were analyzed in detail. The results and implications from this study can provide useful guidance for policymakers to alleviate ozone and haze pollution in Beijing.

2. Methodology

2.1 Field measurement

The sampling site is at the roof of a three-floor building on the campus of Tsinghua University (40.00°N, 116.33°E), northwest of Beijing urban area (Fig. S1). The altitude of the sampling site is 57 m. This sampling site is surrounded by school and there are no large emission sources nearby, therefore it can represent the urban air quality in Beijing. Details of the site description is found in Xu et al., (2019).

The air samples were collected using 6 L summa canisters (Entech, USA) with a stable rate of 4.26 ml/min. The samples were pre-processed to remove N_2, O_2, CO_2, CO and H_2O in the samples and to further concentrate the samples in volume by the cryogenic pre-concentrator (Model 7100, Entech Instruments Inc., USA). Pressure gage was used to test if the canister has air leakage exist before sampling every time, and blanks were prepared using cleaned canisters to fill with high purity nitrogen. The cryotraps of precooling system was baked before analyses each day and between every samples. The VOCs in air samples were analyzed by a gas chromatography system that was equipped with a mass spectrometric detector (GC-MS) (Agilent Tech., 7890/5975, USA). The availability of this system for VOCs measurement are well verified and it has been used in field campaigns (Li

et al., 2014; Wu et al., 2016). The column temperature was controlled by an initial temperature of -40 °C. The programmed temperature was used with helium as carrier gas, and the flow rate was set at 1.5 ml min^{-1}. The initial temperature was set at 90 °C, and then switched to 220 °C. In this work, 95 target VOCs, including 25 alkanes, 8 alkenes, 16 aromatics, 34 halocarbons and 12 OVOC were quantified. It should be noted that VOCs compounds (C2-C3) with low boiling point (i.e., ethane, ethene, acetylene, and propane) were not detected by the GC-MS system. The standard substance (SPECTRA GASES Inc., USA) mentioned for Photochemical Assessment Monitoring Stations (PAMS) and US EPA TO-15 standard was used to construct the calibration curves for the target VOCs. Quality assurance and quality control, including method detection limit (MDL) of each compound, laboratory and field blanks, retention time, accuracy and duplicate measurements of samples were performed according to USEPA Compendium Method TO-15 (USEPA 1999). The correlated coefficients of the calibration curves for all the compounds were > 0.95. The relative standard deviation (RSD) for all of compounds of triplicates were 0.5%-6.0%. Previous field measurements have reported that the precision of GC-MS system for hydrocarbons and aldehydes was below 6% and 15%, respectively (Li et al., 2014; Wu et al., 2016). In this work, one kind of aldehyde substance, i.e., ethylacrolein was detected, with R^2 and RSD of 0.99 and 4.5%, respectively.

During the sampling periods, the measurements of $PM_{2.5}$, gaseous pollutants (NO_X and O_3), and meteorological variables (such as temperature, relative humidity, wind speed, and wind direction) were conducted simultaneously. NO_X and O_3 were analyzed using the Ozone Analyzer (Thermo Fisher Scientific USA, 49I) and NO–NO_2-NO_X Analyzer (Thermo Fisher Scientific USA, 17I), respectively. The mass concentration of $PM_{2.5}$ was measured using an oscillating balance analyzer (TH-2000Z, China) (Wang et al., 2014a). The quality assurance of NO_2, O_3, and $PM_{2.5}$ was conducted based on HJ 630-2011 specifications. Meteorological including

wind speed (WS), wind direction (WD), relative humidity (RH), air pressure, temperature, and precipitation were measured by an automatic weather monitoring system. The planetary boundary height was obtained from the European Centre for Medium-Range Weather Forecasts (https://www.ecmwf.int/en/forestcasts/datasets/browse-reanalysis -datasets).

2.2 Ozone formation potential (OFP) and secondary formation potential (SOAFP) calculation

The formation potential of O_3 and SOA was used to characterize the relative importance of VOCs species and sources in secondary formation, which were estimated using Eqs. (1) and (2).

$$OFP = \sum_{i}^{n} MIR_i \times [VOC(ppb)]_i \quad (1)$$

$$SOAFP = \sum_{i}^{n} Y_i \times [VOC(ppb)]_i \quad (2)$$

where *n* represents the number of VOCs, [VOC]*i* represents the *i*th VOC species concentration, MIR*i* is the maximum incremental reactivity for the *i*th VOC species, and *Yi* is the SOA yield of VOC_i (McDonald et al., 2018). The MIR for each VOC species were taken from the updated Carter research results (http://www.engr.ucr.edu/~carter/reactdat.htm, last access: 24 February 2021). For species lacking yield curves, the fractional aerosol coefficient (FAC) values proposed by Grosjean and Seinfeld (1989) were used.

2.3 Deweathered model

In this work, the influences of meteorological conditions on O_3 and $PM_{2.5}$ were removed using the random forest (RF) model. The meteorological predictors in the RF model include wind speed (*WS*), wind direction (*WD*), air temperature (*T*), relative humidity (*RH*), precipitation (*Prec*), air pressure (*P*), time predictors (year, day of year (*DOY*), hour) and planetary boundary layer height (*BLH*). These meteorological parameters have been reported to be strongly associated with $PM_{2.5}$ and O_3 concentrations in various regions in China (Chen et al., 2020; Feng et al., 2020) and contributed significantly in previous $PM_{2.5}$ and O_3 prediction models (She et al., 2020; Li et al.,

2020). The original dataset was randomly classified into a training dataset (90 % of input dataset) for developing the RF model, and the remaining one was treated as the test dataset. After the building of the RF model, the deweathered technique was applied to predict the air pollutant level at a specific time point. The differences in original pollutant concentrations and deweathered pollutant concentrations were regarded as the concentrations contributed by meteorology. Statistical indicators including R^2, RMSE, and MAE values were regarded as the major criteria to evaluate the modeling performance.

2.4 Positive matrix factorization (PMF)

In this study, the US EPA PMF 5.0 software was used for VOCs source apportionment (Abeleira et al., 2017; Li et al., 2019a; Xue et al., 2017). The detailed description of the PMF model is found elsewhere (Ling et al., 2011; Yuan et al., 2009). PMF uses both concentration and user-provided uncertainty associated with the data to weight individual points. Species with high percentages of missing values (> 40 %) and with signal-to-noise ratio of below 2 were excluded. Based on this, 53 VOC species including source tracers (e.g., chloromethane, trichloroethylene, tetrachloroethylene and MTBE) and SO_2 were chosen for the source apportionment analysis. Data values below the MDL were replaced by MDL/2, and the missing data were substituted with median concentrations. If the concentration is less than or equal to the MDL provided, the uncertainty is calculated using the equation of Unc = 5⁄6 × MDL; if the concentration is greater than the MDL provided, the uncertainty is calculated as Unc = $[(\text{error faction} \times \text{mixing ratio})^2 + (\text{MDL})^2]1/2$.

During the PMF analysis, the bootstraps (BS) method, displacement (DISP) analysis, and the combination of the DISP and BS (BS–DISP) were used to evaluate the uncertainty of the base run solution. A total of 100 bootstrap runs were performed, and acceptable results were gained for all factors (above 90%). Based on the DISP analysis, the observed drop in the *Q* value was below 0.1 %, and no factor swap occurred, confirming that

the solution was stable. The BS–DISP analysis showed that the observed drop in the *Q* value was less than 0.5 %, demonstrating that the solution was useful.

3. Results and discussion

3.1 TVOC mixing ratios and chemical composition

The time series of meteorological parameters and concentrations of air pollutants during the measurement period are shown in Fig. 1. The ambient temperature ranged from -13.3℃ to 38.7℃ and the RH varied between 5% and 99% across the sampling months. Prevailing winds shifted between southwesterly and northeasterly with WS of 0–6.8 m s^{-1}. The mixing ratio of total VOCs (TVOC) ranged from 5.5–118.7 ppbv during the sampling period with relatively higher values during September and November (49.9-51.6 ppbv) while relatively lower values (22.2-27.5 ppbv) across the other months. Major VOC compositions were generally consistent during the whole measurement period. Alkanes, OVOCs and halocarbons were the dominant chemical groups, accounting for 75-81% of the TVOCs across the sampling months. In terms of individual species, acetone, dichloromethane, butane, toluene, methyl tert butyl ether (MTBE), *i*-pentane, propylene, hexane, 1,1- dichloroethane, benzene and 1-butene made up the largest contribution, accounting for 50.6 % of the TVOC on average during the whole measurement period.

The comparison of concentration and composition of chemical groups observed in this work and previous studies is shown in Fig. 2. Clearly, the concentrations of TVOCs and major VOC groups observed in this study were apparently lower than those in 2014 and 2016 in urban sites in Beijing (An et al., 2012; Liu et al., 2020a; Li et al., 2015b), indicating the effectiveness of control measures in most recent years on lowering VOCs emission. Besides, the composition of major chemical groups also showed remarkable changes, with decreased proportions

of alkanes while increased fractions of halocarbons, aromatics and OVOCs, reflecting the changes in emission sources types in most recent years.

During the measurement period, 14 O_3 pollution days (days with maximum 8-h average O_3 exceeding 160 μg m^{-3}) were observed, (i.e., 17-22 April, 3-17 May, 18-29 June, 2-13 July, and 25-29 September of 2019), and April, May, June, July, and September of 2019 were defined as the O_3-polluted months. The comparison of meteorological parameters and trace gases on O_3 pollution and compliance days (days with maximum 8-h average O_3 below 160 μg m^{-3}) of the four O_3-polluted months is shown in Fig. 3. The WS on O_3 pollution days (1.31 ± 0.90 m s^{-1}) was slightly lower than that on O_3 compliance days (1.47 ± 1.10 m s^{-1}), indicating that precursors were more conductive to be diluted on O_3 compliance days. The variation trend of O_3 and temperature displayed the negative correlation, and the linear correlations between O_3 and temperature on O_3 pollution days (R^2 = 0.63) was stronger than that on O_3 compliance days (R^2 = 0.35). The mean TVOC concentration on O_3 pollution days (32.3 ppbv) was higher than that on O_3 compliance days (29.6 ppbv), which was mainly attributed to higher concentrations of MTBE, acrolein, trans-2-butene r on pollution days. MTBE is widely used as a fuel additive in motor gasoline (Liang et al., 2020), and trans-2-butene is the main component of oil/gas evaporation (Li et al., 2019a). Such result suggested enhanced contribution of traffic emissions on O_3 pollution days. Besides, the concentration of isoprene, which is primarily produced by vegetation through photosynthesis, increased significantly on O_3 pollution days probably due to the stronger plant emission at elevated temperature (Guenther et al., 1993, 2012; Stavrakou et al., 2014). The ratio of *m/p*-xylene to ethylbenzene (X/E) measured can be used as an indicator of the photochemical aging of air masses because of their similar sources in urban environments and differences in atmospheric lifetimes (Carter., 2010; Miller et al., 2012; Wang et al., 2013a). The mean X/E

194 value on O_3 compliance days (1.41) was higher than that on O_3 pollution days (1.17), indicating enhanced
195 secondary transformation of VOCs on O_3 pollution days.

196 The daily $PM_{2.5}$ concentrations ranged from 9-260 μg m^{-3} with the mean value of 88.5 μg m^{-3} during the
197 measurement period. 15 $PM_{2.5}$ pollution days (daily average $PM_{2.5}$ exceeding 75 μg m^{-3}) were observed(i.e., 1-2
198 December and 5 December of 2018, 3 January, 12-13 January, 22-23 April, 29 April, 12 May, 15 May, 19 October,
199 and 21-23 November of 2019), and December of 2018, January, Apri, May, October and November of 2019 were
200 identified as the $PM_{2.5}$-polluted months. During the six $PM_{2.5}$-polluted months, , the WS on $PM_{2.5}$ pollution days
201 (1.05 ± 1.06 m s^{-1}) was lower than that on $PM_{2.5}$ compliance days (1.43 ± 1.06 m s^{-1}), indicating the weaker
202 ability of winds for the dilution and diffusion of precursor on $PM_{2.5}$ pollution days. Both the value of relative
203 humidity (RH) and TVOCs increased significantly on $PM_{2.5}$ pollution days, suggesting that the secondary
204 transformation of VOCs was more conducive at higher RH. The mean X/E value on $PM_{2.5}$ compliance days (1.47)
205 was slightly higher than that on $PM_{2.5}$ pollution days (1.44), indicating enhanced secondary transformation of
206 VOCs on $PM_{2.5}$ pollution days.

207 ## 3.2 The role of VOCs on secondary pollution

208 ### 3.2.1 Estimating O_3 and $PM_{2.5}$ levels contributed by emissions

209 O_3 and secondary aerosols are primarily formed via photochemical reactions in the atmosphere, of which
210 concentrations could be largely influenced by meteorological conditions (Chen et al., 2020; Feng et al., 2020;
211 Zhai et al., 2019). In this work, the respective contributions of meteorology and emissions to $PM_{2.5}$ and O_3
212 variations were determined using the RF model as described in section 2.3. The coefficients of determination (R^2)
213 for the RF model in predicting $PM_{2.5}$ and O_3 are 0.85 and 0.91, respectively (Shown in Fig. S2). The respective
214 contributions of anthropogenic and meteorology to O_3 and $PM_{2.5}$ during each period is shown in Fig. 4. During

215 the O_3-polluted months, the meteorologically-driven O_3 level on O_3 pollution days (72.5 μg m^{-3}) was significantly
216 higher than that on O_3 compliance days (35.3 μg m^{-3}). After removing the meteorological contribution, the
217 residual emission-driven O_3 level on O_3 pollution (45.3 μg m^{-3}) and compliance days (44.9 μg m^{-3}) of the O_3-
218 polluted months was almost identical and were significantly higher than that during the non-O_3-polluted months
219 (23.8 μg m^{-3}). The emission-driven $PM_{2.5}$ level was in the order of: $PM_{2.5}$ pollution days of the $PM_{2.5}$-polluted
220 months (55 μg m^{-3}) > $PM_{2.5}$ compliance days of the $PM_{2.5}$-polluted months (44 μg m^{-3}) > non-$PM_{2.5}$-polluted
221 months (29 μg m^{-3}). These results suggested that apart from meteorological factors, emissions also play a role in
222 deteriorating $PM_{2.5}$ and O_3 pollution, and reducing anthropogenic emissions is essential for improving air quality.
223 The VOCs/NO_X ratio has been widely used to distinguish whether the O_3 formation is VOC limited or NO_X
224 limited (Li et al., 2019a). Generally, VOC-sensitive regime occurs when VOCs/NO_X ratios are below 10 while
225 NO_X-sensitive regime occurs when VOCs/NO_X ratios are higher than 20 (Hanna et al., 1996; Sillman, 1999). In
226 this study, the values of VOCs/NO_X (ppbv $ppbv^{-1}$) were all below 3 during both the O_3-polluted and non-O_3-
227 polluted months (Fig. S3), suggesting that the O_3 formation was sensitive to VOCs, and thus the reductions of
228 the emissions of VOCs will be beneficial for O_3 alleviation.

229 **3.2.2 Contribution of VOCs to OFP and SOAFP**

230 As discussed in 3.1, O_3 formation was generally VOCs-sensitive during the measurement period.
231 Quantifying the contribution of speciated VOCs species to O_3 is helpful for developing effective VOCs control
232 measures and alleviating O_3 pollution. The averaged OFP on O_3 pollution days of the O_3-polluted months, O_3
233 compliance days of the O_3-polluted months, and during the non-O_3-polluted months were 224.9, 201.4, and 187.5
234 μg m^{-3}, respectively (Fig. 5). According to our observations, the higher OFP on O_3 pollution days than that on O_3
235 compliance days during the O_3-polluted months was mainly attributed to higher levels of trans-2-butene, o-xylene

and acrolein O_3 on pollution days, in line with that in Fig. 3. Alkenes, aromatics and OVOCs were the three biggest contributors to O_3 formation, accounting for 85.1%, 85.7% and 81.6% of the total OFP on O_3 pollution days of the O_3-polluted months, O_3 compliance days of the O_3-polluted months, and during the non-O_3-polluted months, respectively. In terms of the individual species, the top 10 highest contributors during the O_3-polluted months were toluene (7.5% and 6.4% on O_3 compliance and polluted days, respectively), trans-2-butene (7.5% and 9.6%), acrolein (5.7% and 10.8%), m/p-xylene (6.9% and 6.1%), o-xylene (5.8% and 6.6%), 1-butene (7.1% and 5.2%), 1-hexene (5.4% and 4.4%), vinyl acetate (5.7% and 4.2%), methyl methacrylate (4.8% and 5.5%), and 1-pentene (4.4% and 4.5%). During the non-O_3-polluted months, the overall OFP was mainly contributed by toluene (10.8%), trans-2-butene (10.5%), 1-butene (7.3%), m/p-xylene (6.5%), 1-pentene (5.7%), 1-hexene (5.0%), methyl methacrylate (4.9%), o-xylene (4.9%), vinyl acetate (3.8%), and isopentane (2.3%), respectively.

As shown in Fig. S3, the ratio of VOCs/NOx was generally below 3 during the sampling period, indicating high NO_X conditions. Based on the estimated yields of the VOCs shown in Table S2, the SOAFPs were calculated and compared in Fig. 5. The mean SOAFP on $PM_{2.5}$ pollution days of the $PM_{2.5}$-polluted months, $PM_{2.5}$ compliance days of the $PM_{2.5}$-polluted months, and during the non-$PM_{2.5}$-polluted months were 1.28, 1.07, and 0.89 μg m^{-3}. During the six $PM_{2.5}$-polluted months, the higher SOAFP on $PM_{2.5}$ pollution days than that on $PM_{2.5}$ compliance days was mainly attributed to higher levels of 1,2,4-trimethylbenzene, n-undecanone, n-Nonane, 1,4-diethylbenzene, and 1,3-diethylbenzene on $PM_{2.5}$ pollution days. Aromatics have the largest SOAFP, accounting for 74% and 75% of the total SOAFP on $PM_{2.5}$ pollution and compliance days of the $PM_{2.5}$-polluted months, and 70% of the total SOAFP during the non-$PM_{2.5}$-polluted months, respectively. The 10 species responsible for most of the SOAFP were toluene (41% and 40% on $PM_{2.5}$ pollution and compliance days of the $PM_{2.5}$-polluted months, and 33% during the non-$PM_{2.5}$-polluted months), 1-hexene (13.0%, 12.5%, and 15.2%), xylenes (11.6%, 14.1%

and 14.8%), ethylbenzene (4.9%, 5.3% and 6.0%), styrene (4.5%, 5.6% and 5.6%), 1-pentene (3.3%, 3.4% and 4.3%), methyl cyclopentane (2.1%, 2.7% and 3.6%), 1,2,3-trimethylbenzene (2.8%, 2.4% and 2.8%), m-ethyl toluene (1.7%, 1.4% and 1.7%) and p-ethyl toluene (1.7%, 1.4% and 1.7%), respectively.

3.3 Source apportionment of VOCs

3.3.1 Indication from tracers

The great changes in the mixing ratios of VOCs species are mainly affected by the photochemical processing and the emission inputs, and ambient ratios for VOCs species having similar atmospheric lifetimes are indicators of different sources (Li et al., 2019a; Raysoni et al., 2017 Song et al., 2021). The ratio of *i*-pentane to *n*-pentane are widely used to examine the impact of vehicle emissions, fuel evaporation and combustion emissions, within the i/n-pentane ratios of ranging between 2.2–3.8, 1.8–4.6 and 0.56-0.80, respectively (McGaughey et al., 2004; Jobson et al., 2004; Russo et al., 2010; Wang et al., 2013b; Yan et al., 2017). As shown in Fig. 6, the i/n-pentane ratios during the $PM_{2.5}$-polluted months were mostly within the range of 0.3-2.0, suggesting the pentanes were from the mixed sources of coal combustion and fuel evaporation. During the non-$PM_{2.5}$-polluted months, the i/n-pentane ratios were distributed in the range of 1.3-3.4, indicating strong impacts from vehicle exhaust and fuel evaporation. During the O_3-polluted months, most of the i/n-pentane ratios (1.5-2.5) were distributed within the reference range of vehicle exhaust and fuel evaporation, whereas most of the i/n-pentane ratios during the non-O_3-polluted months ranged between 1.7-2.1, suggesting the significant impact of fuel evaporation.

The toluene/benzene (T/B) ratio, a widely used indicator for sources of aromatics. In areas heavily impacted by vehicle emissions, the T/B ratio lies in the range of 0.9–2.2 (Qiao et al., 2012; Dai et al., 2013; Wang et al., 2013c; Yao et al., 2013; Zhang et al., 2013; Yao et al., 2015a; Mo et al., 2016; Deng et al., 2018). Higher T/B ratios were reported for solvent use (greater than 8.8) (Yuan et al., 2010; Wang et al.,2014b; Zheng et al., 2013)

278 and industrial processes (1.4-5.8) (Mo et al., 2015; Shi et al.,2015). In burning source emission studies, the T/B
279 ratio was below 0.6 in different combustion process and raw materials (Tsai et al., 2003; Akagi et al., 2011; Mo
280 et al., 2016). Most of the T/B ratios during the $PM_{2.5}$-polluted and non-$PM_{2.5}$-polluted months were within the
281 range of 1.1-1.8 and 0.8-2.2, whereas the T/B ratios were mostly distributed within the range of 0.8-2.2 and 0.9-
282 1.9 during the O_3-polluted and non-O_3-polluted months, respectively, suggesting the significant impact of vehicle
283 and industrial emissions.

284 **3.3.2 PMF**

285 The factor profiles given by PMF and the contribution of each source to ambient VOCs during each period
286 is presented in Fig. 7 and Fig. 8, respectively. Six emission sources were identified: coal/biomass burning, solvent
287 use, industrial sources, oil gas evaporation, gasoline vehicle emission, and diesel vehicle emission based on the
288 corresponding markers for each source category. In general, diesel vehicle exhaust, gasoline vehicle exhaust and
289 industrial emissions were the main VOCs sources during both the O_3-polluted and $PM_{2.5}$-polluted months, with
290 total contributions of 62% and 62% on O_3 pollution and compliance days of the O_3-polluted months, and 66%
291 and 59% on $PM_{2.5}$ pollution and compliance days of the $PM_{2.5}$-polluted months, respectively. The O_3-polluted
292 months exhibited higher proportions of diesel (24% on O_3 compliance days and 27% on O_3 pollution days) and
293 gasoline vehicle emission (17% on O_3 compliance days and 16% on O_3 pollution days) compared with the non-
294 O_3-polluted months (8% and 13%, respectively). During the O_3-polluted months, the contributions of industrial
295 emissions (22%) and fuel evaporation (18%) on O_3 pollution days were much higher than those on O_3 compliance
296 days (18% and 13%, respectively). Figure 9 presents the relative contributions of individual VOC sources from
297 PMF to OFP. On the base of O_3 formation impact, diesel and gasoline vehicle exhaust were major contributors.
298 During the O_3-polluted months, vehicle emissions and fuel evaporation showed higher OFP values on O_3

299 pollution days (93.9 and 35.5 μg m^{-3}) compared with those on O_3 compliance days (88.0 and 25.8 μg m^{-3},
300 respectively). Although industrial emissions act as an important source for VOCs concentrations on O_3-pollution
301 days (shown in Fig. 8), the potential to form O_3 is limited, accounting for 11% of the total OFP. As illustrated in
302 Fig.7, the industrial source was distinguished by high compositions of alkanes while relatively lower
303 compositions of alkenes and aromatics, resulting in low O_3 formation potentials. Such results suggested that the
304 fuel use and diesel vehicle exhaust should be controlled preferentially for O_3 mitigation.

305 The $PM_{2.5}$-polluted months showed higher proportions of industrial (29% on both $PM_{2.5}$ compliance and
306 $PM_{2.5}$ pollution days) and coal/biomass combustion emissions (16% on $PM_{2.5}$ compliance days and 18% on $PM_{2.5}$
307 pollution days) compared with the non-$PM_{2.5}$-polluted months (17% and 10%, respectively). The $PM_{2.5}$ pollution
308 days were dominated by industrial emission (29%), diesel vehicle exhaust (24%), and combustion source (18%).
309 During the $PM_{2.5}$-polluted months, the contribution of diesel vehicle exhaust on $PM_{2.5}$ pollution days (24%) was
310 higher than that on $PM_{2.5}$ compliance days (16%). On the base of $PM_{2.5}$ formation impact, diesel vehicle exhaust
311 and combustion were two major contributors on $PM_{2.5}$ pollution days (shown in Fig. 9), and these two sources
312 showed obvious higher SOAFP on $PM_{2.5}$ pollution days (0.30 and 0.32 μg m^{-3}, respectively) compared with those
313 on $PM_{2.5}$ compliance days of the $PM_{2.5}$-polluted months (0.15 and 0.14 μg m^{-3}, respectively). Although industrial
314 emissions act as an important source for VOCs concentrations on $PM_{2.5}$pollution days, the potential to form $PM_{2.5}$
315 is limited, accounting for 16% of the total SOAFP. The above results suggested that diesel vehicle exhaust and
316 combustion should be controlled preferentially for alleviating $PM_{2.5}$ pollution.

317 Based on the mass concentrations of individual species in each source, m/p-xylene, o-xylene, methyl
318 methacrylate, vinyl acetate, 1-hexene, and acrolein in gasoline and diesel vehicular emissions; toluene, trans-2-
319 butene, and 1-pentene in fuel evaporation and diesel vehicular emissions; acrolein in solvent, gasoline vehicular

and diesel vehicular emissions were the dominant species contributing to photochemical O_3 formation (Fig. 10). Toluene, m/p-xylene, o-xylene, styrene, ethylbenzene, 1-pentene, 1,2,3-trimethylbenzene from combustion and diesel vehicular emissions; 1-hexene from diesel vehicular emission; and methyl cyclopentane from combustion, industrial and diesel vehicular emissions were the dominant contributors for SOA formation during the $PM_{2.5}$ pollution periods (Fig. 10).

4. Conclusions

In this work, the field sampling campaign of VOCs was conducted at urban Beijing during December 2018 and November 2019. The VOCs concentrations ranged from 5.5 to 118.7 ppbv with mean value of 34.9 ppbv. Alkanes, OVOCs and halocarbons were the dominant chemical groups, accounting for 75-81% of the TVOCs across the sampling months. By excluding the meteorological impact, the emission-driven O_3 level during the O_3-polluted months were higher than that during the non-O_3-polluted months, and similar pattern was found for $PM_{2.5}$. The molar ratio of VOCs to NO_X indicated that O_3 formation was limited by VOCs during both the O_3-polluted non-O_3-polluted months, and thus reducing VOCs emission is essential for alleviation of O_3 pollution. The contributions of coal/biomass combustion, solvent use, industrial sources, oil/gas evaporation, gasoline exhaust, and diesel exhaust were identified based on PMF analysis. Considering both the concentration and maximum incremental reactivity of individual VOC species for each source, fuel use and diesel exhaust sources were identified as the main contributors of O_3 formation during the O_3-polluted months, particularly the VOCs species of toluene, xylenes, trans-2-butene, acrolein, methyl methacrylate, vinyl acetate, 1-butene and 1-hexene, illustrating the necessity of conducting emission controls on these pollution sources and species for alleviating O_3 pollution. VOCs from diesel vehicles and combustion were found to be the dominant contributors for SOAFP,

particularly the VOC species of toluene, 1-hexene, xylenes, ethylbenzene and styrene, and top priority should be given to these for the alleviation of haze pollution.

Acknowledgements

This work was supported by the National Natural Science Foundation of China (92044302) and the Beijing Municipal Science and Technology Project (Z211100004321006 & Z191100009119001).

Data availability

The meteorological data are available at http: //data.cma.cn/ (China Meteorological Administration). The website can be browsed in English http://data.cma.cn/en. The concentrations of air pollutants including $PM_{2.5}$, O_3 and NO_X are available at https://air.cnemc.cn:18007/ (Ministry of Ecology and Environment the People's Republic of China). The website can be browsed in English http://english.mee.gov.cn/.

References Abeleira, A., Pollack, I. B., Sive, B., Zhou, Y., Fischer, E. V., Farmer, D. K., 2017. Source characterization of volatile organic compounds in the Colorado Northern Front Range Metropolitan Area during spring and summer 2015, J. Geophys. Res.-Atmos., 122, 3595–3613, https://doi.org/10.1002/2016jd026227.

Ahmad, W., Coeur, C., Tomas, A., Fagniez, T., Brubach, J. B., Cuisset, A., 2017. Infrared spectroscopy of secondary organic aerosol precursors and investigation of the hygroscopicity of SOA formed from the OH reaction with guaiacol and syringol. Appl. Opt. 56, E116, https://doi.org/10.1364/AO.56.00E116.Akagi, S. K., Yokelson, R. J., Wiedinmyer, C., Alvarado, M. J.,Reid, J. S., Karl, T., Crounse, J. D., Wennberg, P. O., 2011. Emission factors for open and domestic biomass burning for usein atmospheric models. Atmos. Chem. Phys. 11, 4039–4072.

Atkinson, R., 2000. Atmospheric chemistry of VOCs and NO_X. Atmos. Environ. 34, 2063–2101.

An, J.L., Wang, Y.S., Wu, F.K., Zhu, B., 2012. Characterizations of volatile organic compounds during high ozone episodes in Beijing, China. Environ. Monit. Assess. 184, 1879e1889.

Carter, W.P.L. and Atkinson, R., 1989. Computer modeling study of incremental hydrocarbon reactivity. Environ. Sci. Technol. 23, 864–880, https://doi.org/10.1021/es00065a017.

Carter, W.P.L., 2010. Development of the SAPRC-07 chemical mechanism, Atmos. Environ. 44, 5324–5335, https://doi.org/10.1016/j.atmosenv.2010.01.026.

Chang, T.Y. and Rudy, S.J., 1990. Ozone-forming potential of organic emissions from alternative-fueled vehicles, Atmos. Environ., 24, 2421–2430, https://doi.org/10.1016/0960-1686(90)90335-K.

Chen, L., Zhu, J., Liao, H., Yang, Y., Yue, X., 2020. Meteorological influences on $PM_{2.5}$ and O_3 trends and associated health burden since China's clean air actions, Sci. Total Environ. 744, 140837, https://doi.org/10.1016/j.scitotenv.2020.140837.

Dai, P., Ge, Y., Lin, Y., Su, S., and Liang, B., 2013. Investigation on characteristics of exhaust and evaporative emissions from passenger cars fueled with gasoline/methanol blends. Fuel. 113, 10–16.

Deng, C. X., Jin, Y. J., Zhang, M., Liu, X. W., Yu, Z.M., 2018. Emission Characteristics of VOCs from On-Road Vehicles in an Urban Tunnel in Eastern China and Predictions for 2017–2026. Aerosol Air Qual. Res. 18, 3025–3034.

Doumbia, T., Granier, C., Elguindi, N., Bouarar, I., Darras, S., Brasseur, G., Gaubert, B., Liu, Y., Shi, X., Stavrakou, T., Tilmes, S., Lacey, F., Deroubaix, A., Wang, T., 2021. Changes in global air pollutant emissions during the COVID-19 pandemic: a dataset for atmospheric modeling. Earth Syst. Sci. Data. 13, 4191–4206.

Fan, H., Zhao, C., Yang, Y., 2020. A Comprehensive Analysis of the Spatio-Temporal Variation of Urban Air Pollution in China During 2014–2018, Atmos. Environ., 220, 117066, https://doi.org/10.1016/j.atmosenv.2019.117066.

Feng, J., Liao, H., Li, Y., Zhang, Z., Tang, Y., 2020. Long-term trends and variations in haze-related weather conditions in north China during 1980–2018 based on emission-weighted stagnation intensity. Atmos. Environ. 240, 117830, https://doi.org/10.1016/j.atmosenv.2020.117830.

Fu, Y., Liao, H., Yang, Y., 2019. Interannual and Decadal Changes in Tropospheric Ozone in China and the Associated Chemistry Climate Interactions: A Review, Adv. Atmos. Sci. 36, 975–993.

Gani, S., Bhandari, S., Seraj, S., Wang, D. S., Patel, K., Soni, P., Arub, Z., Habib, G., Hildebrandt Ruiz, L., Apte, J. S., 2019. Submicron aerosol composition in the world's most polluted megacity: the Delhi Aerosol Supersite study. Atmos. Chem. Phys. 19, 6843–6859.

Grosjean, D., and Seinfeld, J. H., 1989. Parameterization of the formation potential of secondary organic aerosols, Atmos. Environ., 23, 1733-1747, 10.1016/0004- 6981(89)90058-9.

Guenther, A.B., Zimmerman, P.R., Harley, P.C., Monson, R.K., Fall, R., 1993. Isoprene and monoterpene emission rate variability: Model evaluations and sensitivity analyses. J. Geophys. Res. Atmos. 98, 12609–12617, https://doi.org/10.1029/93JD00527.

Han, S., Zhao, Q., Zhang, R., Liu, Y., Li, C., Zhang, Y., Li, Y., Yin, S., Yan, Q., 2020. Emission characteristic and environmental impact of process-based VOCs from prebaked anode manufacturing industry in Zhengzhou, China. Atmos. Pollut. Res. 627 11, 67-77, 10.1016/j.apr.2019.09.016.

Hanna, S. R., Moore, G. E., Fernau, M., 1996. Evaluation of photochemical grid models (UAM-IV, UAM-V, and the ROM/UAMIV couple) using data from the Lake Michigan Ozone Study (LMOS). Atmos. Environ. 30, 3265–3279.

Hong, Z., Li, M., Wang, H., Xu, L., Hong, Y., Chen, J., Chen, J., Zhang, H., Zhang, Y., Wu, X., Hu, B., Li, M., 2019. Characteristics of atmospheric volatile organic compounds (VOCs) at a mountainous forest site and two urban sites in the southeast of China. Sci. Total. Environ. 657, 1491–1500, https://doi.org/10.1016/j.scitotenv.2018.12.132.

Huang, R.J., Zhang, Y., Bozzetti, C., Ho, K.F., Cao, J.J., Han, Y., Daellenbach, K. R., Slowik, J. G., Platt, S. M., Canonaco, F., Zotter, P., Wolf, R., Pieber, S. M., Bruns, E. A., Crippa, M., Ciarelli, G., Piazzalunga, A., Schwikowski, M., Abbaszade, G., Schnelle-Kreis, J., Zimmermann, R., An, Z., Szidat, S., Baltensperger, U., El Haddad, I., Prevot, A.S.H., 2014. High secondary aerosol contribution to particulate pollution during haze events in China, Nature, 514, 218-222, 10.1038/nature13774.

Jobson, B. T., Berkowitz, C. M., Kuster, W. C., Goldan,P. D., Williams, E. J., Fesenfeld, F. C., Apel, E. C.,Karl, T., Lonneman, W. A., Riemer, D., 2004. Hydrocarbon source signatures in Houston, Texas: Influence of the petrochemical industry. J. Geophys. Res. Atmos. 109, D24305, https://doi.org/10.1029/2004jd004887.

Kuang, Y., He, Y., Xu, W.Y., Yuan, B., Zhang, G., Ma, Z.Q., Wu, C.H., Wang, C.M., Wang, S.H., Zhang, H.Y., Tao, J.C., Ma, N., Su, H., Cheng, Y.F., Shao, M., Sun, Y.L., 2020. Environ Sci & Techno**.** *54* (7), 3849-3860.

Li, L., Chen, Y., Zeng, L., Shao, M., Xie, S., Chen, W., Lu, S., Wu, Y., Cao, W., 2014. Biomass burning contribution to ambient volatile organic compounds (VOCs) in the Chengdu–Chongqing Region (CCR), China. Atmos. Environ. 99, 403–410.

Li, J., Xie, S.D., Zeng, L.M., Li, L.Y., Li, Y.Q., Wu, R.R., 2015. Characterization of ambient volatile organic compounds and their sources in Beijing, before, during, and after Asia-Pacific Economic Cooperation China 2014. Atmos. Chem. Phys.15, 7945–7959

Li, G., Bei, N., Cao, J., Wu, J., Long, X., Feng, T., Dai, W., Liu, S., Zhang, Q., Tie, X., 2017a. Widespread and persistent ozone pollution in eastern China during the non-winter season of 2015: observations and source attributions, Atmos. Chem. Phys., 17, 2759–2774, https://doi.org/10.5194/acp-17-2759-2017.

Li, Y. J., Sun, Y., Zhang, Q., Li, X., Li, M., Zhou, Z., Chan, C. K., 2017b. Real-time chemical characterization of atmospheric particulate matter in China: A review, Atmos. Environ., 158, 270–304.

Li, B., Ho, S.S.H., Gong, S., Ni, J., Li, H., Han, L., Yang, Y., Qi, Y., Zhao, D., 2019a. Characterization of VOCs and their related atmospheric processes in a central Chinese city during severe ozone pollution periods. Atmos. Chem & Phys. 19, 617-638.

Li, K., Jacob, D.J., Liao, H., Shen, L., Zhang, Q., Bates, K.H., 2019c. Anthropogenic Drivers of 2013−2017 Trends in Summer Surface Ozone in China. Proc. Natl. Acad. Sci. 116, 422−427.

Li, K., Li, J., Tong, S., Wang, W., Huang, R.-J., Ge, M., 2019d. Characteristics of wintertime VOCs in suburban and urban Beijing: concentrations, emission ratios, and festival effects. Atmos. Chem & Phys. 19, 8021-8036.

Li, K., Jacob, D.J., Shen, L., Lu, X., De Smedt, I., Liao, H., 2020. Increases in surface ozone pollution in China

from 2013 to 2019: anthropogenic and meteorological influences. Atmos. Chem & Phys. 20, 11423-11433.

Liang, Y., Liu，X., Wu，F., Guo, Y., Xiao, H., 2020. The year-round variations of VOC mixing ratios and their sources in Kuytun City (northwestern China), near oilfields. Atmos. Pollut. Res. 11,9 DOI:10.1016/j.apr.2020.05.022.

Liu, B., Liang, D., Yang, J., Dai, Q., Bi, X., Feng, Y., Yuan, J., Xiao, Z., Zhang, Y., Xu, H., 2016a. Characterization and source apportionment of volatile organic compounds based on 1-year of observational data in Tianjin, China. Environ. Pollut. 218, 757–769, https://doi.org/10.1016/j.envpol.2016.07.072.

Liu, B. S., Liang, D. N., Yang, J. M., Dai, Q. L., Bi, X. H., Feng, Y. C., Yuan, J., Xiao, Z. M., Zhang, Y. F., and Xu, H., 2019b. Characterization and source apportionment of volatile organic compounds based on 1-year of observational data in Tianjin, China. Environ. Pollut. 218, 757–769.

Liu, Y., Wang, H., Jing, S., Gao, Y., Peng, Y., Lou, S., Cheng, T., Tao, S., Li, L., Li, Y., 2019. Characteristics and sources of volatile organic compounds (VOCs) in Shanghai during summer: Implications of regional transport. Atmospheric Environment 215, 116902.

Liu, Y.F., Song, M.D., Liu, X.G., Zhang, Y.P., Hui, L.R., Kong, L.W., Zhang, Y.Y., Zhang, C., Qu, Y., An, J.L., Ma, D.P., Tan, Q.W., Feng, M., 2020a. Characterization and sources of volatile organic compounds (VOCs) and their related changes during ozone pollution days in 2016 in Beijing, China. Environ Pollut. 257, 113599.

Liu, Y.M., Wang, T., 2020b. Worsening urban ozone pollution in China from 2013 to 2017–Part 2: The effects of emission changes and implications for multi-pollutant control. Atmos. Chem. Phys. 20, 6323–6337.

Liu, C., Shi, K., 2021. A review on methodology in O3-NOx-VOC sensitivity study. Environmental pollution, 118249.

Lu, X., Zhang, L., Wang, X., Gao, M., Li, K., Zhang, Y., Yue, X., Zhang, Y., 2020. Rapid increases in warm-

455 season surface ozone and resulting health impact in China since 2013. Environ. Sci & Technol Lett. 7, 240-247.
456 McDonald, B.C., de Gouw, J.A., Gilman, J.B., Jathar, S.H., Akherati, A., Cappa, C.D., Jimenez, J.L., Lee-Taylor,
457 J., Hayes, P.L., McKeen, S.A., Cui, Y.Y., Kim, S.W., Gentner, D.R., Isaacman-VanWertz, G., Goldstein, Allen
458 H., Harley, R.A., Frost, G.J., Roberts, J. M., Ryerson, T.B., Trainer, M., 2018. Volatile chemical products
459 emerging as largest petrochemical source of urban organic emissions, Science, 359, 760,
460 https://doi.org/10.1126/science.aaq0524.
461 McGaughey, G. R., Desai, N. R., Allen, D. T., Seila, R.L., Lonneman, W. A., Fraser, M. P., Harley, R. A., Pollack,
462 A. K., Ivy, J. M., Price, J. H., 2004. Analysis of motor vehicle emissions in a Houston tunnel during the TexasAir
463 Quality Study 2000. Atmos. Environ. 38, 3363 – 3372.
464 Miller, L., Xu, X., Grgicak-Mannion, A., Brook, J., Wheeler, A., 2012. Multi-season, multiyear concentrations
465 and correlations amongst the BTEX group of VOCs in an urbanized industrial city. Atmos. Environ. 61, 305–
466 315.
467 Mo, Z., Shao, M., Lu, S., Qu, H., Zhou, M., Sun, J., Gou, B., 2015. Process-specific emission characteristics of
468 volatile organic compounds (VOCs) from petrochemical facilities in theYangtze River Delta, China. Sci. Total
469 Environ. 533, 422–431.
470 Mo, Z., Shao, M., Lu, S., 2016. Compilation of a source profile database for hydrocarbon and OVOC emissions
471 in China. Atmos. Environ. 143, 209–217.
472 Odum, J.R., Jungkamp, T.P.W., Griffifin, R.J., Flagan, R.C., Seinfeld, J.H., 1997. The atmospheric aerosol-
473 forming potential of whole gasoline vapor. Science. 276, 96–99.
474 Peng, J., Hu, M., Shang, D., Wu, Z., Du, Z., Tan, T., Wang, Y., Zhang, F., Zhang, R., 2021. Explosive secondary
475 aerosol formation during severe haze in the North China Plain. Environ Sci & Technol. 55, 2189-2207.

476 Polissar, A.V., Hopke, P.K., Paatero, P., Kaufmann, Y.J., Hall, D.K., Bodhaine, B.A., Dutton, E.G., Harris, J.M.,
477 1999. The aerosol at Barrow, Alaska: long-term trends and source locations. Atmos. Environ. 33, 2441–2458,
478 https://doi.org/10.1016/S1352- 2310(98)00423-3, 1999.
479 Qiao, Y.Z., Wang, H.L., Huang, C., Chen, C.H., Su, L.Y., Zhou, M., Xu, H., Zhang, G.F., Chen, Y.R., Li, L., Chen,
480 M.H., Huang, H.Y., 2012. Source Profile and Chemical Reactivity of VolatileOrganic Compounds from Vehicle
481 Exhaust. Huanjing Kexue. 33,1071–1079.
482 Raysoni, A.U., Stock, T.H., Sarnat, J.A., Chavez, M.C., Sarnat, S.E., Montoya, T., Holguin, F., Li, W.W., 2017.
483 Evaluation of VOC concentrations in indoor and outdoor microenvironments at near-road schools. Environ.
484 Pollut. 231, 681–693.
485
486 Russo, R. S., Zhou, Y., White, M. L., Mao, H., Talbot, R., Sive, B. C., 2010. Multi-year (2004–2008) record of
487 nonmethane hydrocarbons and halocarbons in New England: seasonal variations and regional sources. Atmos.
488 Chem. Phys. 10, 4909–4929.
489 Sato, K., Takami, A., Isozaki, T., Hikida, T., Shimono, A., Imamura, T., 2010. Mass spectrometric study of
490 secondary organic aerosol formed from the photo-oxidation of aromatic hydrocarbons. Atmos. Environ. 44,
491 1080–1087, https://doi.org/10.1016/j.atmosenv.2009.12.013.
492 Shao, M., Zhang, Y., Zeng, L., Tang, X., Zhang, J., Zhong, L., Wang, B., 2009. Ground-level ozone in the Pearl
493 River Delta and the roles of VOC and NOx in its production. J. Environ. Manage. 90, 512-518.
494 She, Q., Choi, M., Belle, J. H., Xiao, Q., Bi, J., Huang, K., Meng, X., Geng, G., Kim, J., He, K., Liu, M., Liu, Y.,
495 2020. Satellite-based estimation of hourly PM2.5 levels during heavy winter pollution episodes in the Yangtze
496 River Delta, China. Chemosphere. 239, 124678, https://doi.org/10.1016/j.chemosphere.2019.124678.

Shen, L., Jacob, D. J., Liu, X., Huang, G., Li, K., Liao, H., Wang, T, 2019. An evaluation of the ability of the Ozone Monitoring Instrument (OMI) to observe boundary layer ozone pollution across China: application to 2005–2017 ozone trends. Atmos. Chem. Phys. 19, 6551–6560, https://doi.org/10.5194/acp-19-6551-2019.

Shen, L., Wang, Z., Cheng, H., Liang, S., Xiang, P., Hu, K., Yin, T., Yu, J., 2020. A Spatial-Temporal Resolved Validation of Source Apportionment by Measurements of Ambient VOCs in Central China, Int. J. Env. Res. Pub. He. 17, 791, https://doi.org/10.3390/ijerph17030791.

Shi, J., Deng, H., Bai, Z., Kong, S., Wang, X., Hao, J., Han, X., Ning, P., 2015. Emission and profile characteristic of volatile organic compounds emitted from coke production, iron smelt, heating station and power plant in Liaoning Province, China. Sci. Total Environ. 515, 101–108.

Sillman, S., 1999. The relation between ozone, NOx and hydrocarbons in urban and polluted rural environments, Atmos. Environ., 33, 1821–1845, 1999.

Sindelarova, K., Markova, J., Simpson, D., Huszar, P., Karlicky, J., Darras, S., Granier, C., 2022. High-resolution biogenic global emission inventory for the time period 2000–2019 for air quality modelling. Earth Syst. Sci. Data. 14, 251–270.

Sinha, B.P. and Sinha, V., 2019. Source apportionment of volatile organic compounds in the northwest Indo-Gangetic Plain using a positive matrix factorization model. Atmos. Chem. Phys. 19, 15467–15482.

Song, M.D., Li, X., Yang, S.D., Yu, X.A., Zhou, S.X., Yang, Y.M., Chen, S.Y., Dong, H.B., Liao, K.R., Chen, Q., Lu, K.D., Zhang, N.N., Cao, J.J., Zeng, L.M., Zhang, Y.H., 2021. Spatiotemporal variation, sources, and secondary transformation potential of volatile organic compounds in Xi'an, China. Atmos. Chem. Phys. 21, 4939–4958.

517 Stavrakou, T., Müller, J.-F., Bauwens, M., De Smedt, I., Van Roozendael, M., Guenther, A., Wild, M., Xia, X.,
518 2014. Isoprene emissions over Asia 1979–2012: impact of climate and land-use changes. Atmos. Chem. Phys.
519 14, 4587–4605, https://doi.org/10.5194/acp-14-4587-2014.
520 Sun, W., Wang, D., Yao, L., Fu, H., Fu, Q., Wang, H., Li, Q., Wang, L., Yang, X., Xian, A. (2019) Chemistry-
521 triggered events of $PM_{2.5}$ explosive growth during late autumn and winter in Shanghai, China. Environmental
522 pollution. 254, 112864.
523 Sun, Y. L., He, Y., Kuang, Y.. Xu, W. Y., Song, S. J., Ma, N., Tao, J. C., Cheng, P., Wu, C., Su, H., Cheng, Y. F.,
524 Xie, C. H., Chen, C., Lei, L., Qiu, Y. M., Fu, P. Q., Croteau, P., Worsnop, D. R., 2020. Chemical Differences
525 Between PM_1 and $PM_{2.5}$ in Highly Polluted Environment and Implications in Air Pollution Studies. Geophys.
526 Res. Lett. 47, No. e2019GL086288.
527 Tsai, S. M., Zhang, J. J., Smith, K. R., Ma, Y., Rasmussen, R. A., Khalil, M. A. K., 2003. Characterization of
528 Non-methane Hydrocarbons Emitted from Various Cookstoves Used in China. Environ. Sci. Technol. 37, 2869–
529 2877.
530 Tong, Y., Pospisilova, V., Qi, L., Duan, J., Gu, Y., Kumar, V., Rai, P., Stefenelli, G., Wang, L., Wang, Y., Zhong,
531 H., Baltensperger, U., Cao, J., Huang, R.J., Prévôt, A. S. H., Slowik, J. G., 2021. Quantification of solid fuel
532 combustion and aqueous chemistry contributions to secondary organic aerosol during wintertime haze events in
533 Beijing. Atmos. Chem. Phys. 21, 9859−9886.
534 Wang, H.L., Chen, C.H., Wang, Q., Huang, C., Su, L.Y., Huang, H.Y., Lou, S.R., Zhou, M., Li, L., Qiao, L.P.,
535 Wang, Y.H., 2013a. Chemical loss of volatile organic compounds and its impact on the source analysis through
536 a two-year continuous measurement. Atmos. Environ. 80, 488–498.

537 Wang, M., Shao, M., Lu, S.H., Yang, Y.D., Chen, W.T., 2013b. Evidence of coal combustion contribution to
538 ambient VOCs during winter in Beijing. Chin. Chem. Lett. 24, 829–832.
539 Wang, J., Jin, L., Gao, J., Shi, J., Zhao, Y., Liu, S., Jin, T., Bai, Z., Wu, C.Y., 2013c. Investigation of speciated
540 VOC in gasoline vehicular exhaust under ECE and EUDC test cycles. Sci. Total Environ. 445, 110–116.
541 Wang, Y.S., Yao, L., Wang, L.L., Liu, Z.R., Ji, D.S., Tang, G. Q., Zhang, J.K., Sun, Y., Hu, B., Xin, J.Y., 2014a.
542 Mechanism for the formation of the January 2013 heavy haze pollution episode over central and eastern China.
543 Sci. China Earth Sci. 57, 14–25, https://doi.org/10.1007/s11430-013-4773-4.
544 Wang, H., Qiao, Y., Chen, C., Lu, J., Dai, H., Qiao, L., Lou, S., Huang, C., Li, L., Jing, S., Wu, J., 2014b. Source
545 Profiles and Chemical Reactivity of Volatile Organic Compounds from SolventUse in Shanghai, China. Aerosol
546 Air Qual. Res. 14, 301–310.
547 Wang, T., Xue, L., Brimblecombe, P., Lam, Y.F., Li, L., Zhang, L., 2017. Ozone Pollution in China: A Review
548 of Concentrations, Meteorological Influences, Chemical Precursors, and Effects. Sci. Total Environ. 575,
549 1582−1596.
550 Wang, J., Yang, Y., Zhang, Y., Niu, T., Jiang, X., Wang, Y., Che, H., 2019. Influence of meteorological
551 conditions on explosive increase in O3 concentration in troposphere. Sci.Total Environ. 652, 1228-1241.
552 Wang, M, L., Li, S.Y., Zhu, R.C., Zhang, R.Q., Zu, L., Wang, Y.J., Bao, X.F., 2020. On-road tailpipe emission
553 characteristics and ozone formation potentials of VOCs from gasoline, diesel and liquefied petroleum gas fueled
554 vehicles. Atmos. Environ. 223, 117294.
555 Warneke, C., McKeen, S. A., de Gouw, J. A., Goldan, P. D., Kuster, W. C., Holloway, J. S., Williams, E. J.,
556 Lerner, B. M., Parrish, D. D., Trainer, M., Fehsenfeld, F. C., Kato, S., Atlas, E. L., Baker, A., Blake, D. R., 2007.

Determination of urban volatile organic compound emission ratios and comparison with an emissions database. J. Geophys. Res. 112, D10S47, https://doi.org/10.1029/2006jd007930.

Wu, R.R., Li, J., Hao, Y.F., Li, Y.Q., Zeng, L.M., Xie, S.D., 2016. Evolution process and sources of ambient volatile organic compounds during a severe haze event in Beijing, China. Sci. Total. Environ. 560-561, 62-72.

Wu, R. and Xie, S., 2018. Spatial Distribution of Secondary Organic Aerosol Formation Potential in China Derived from Speciated Anthropogenic Volatile Organic Compound Emissions, Environ. Sci. Technol. 52, 8146–8156, https://doi.org/10.1021/acs.est.8b01269.

Xing, J., Wang, S. X., Jang, C., Zhu, Y., Hao, J. M., 2011. Nonlinear response of ozone to precursor emission changes in China: a modeling study using response surface methodology. Atmos. Chem. Phys. 11, 5027–5044.

Xu, W., Sun, Y., Wang, Q., Zhao, J., Wang, J., Ge, X., Xie, C., Zhou, W., Du, W., Li, J., Fu, P., Wang, Z., Worsnop, D.R., Coe, H., 2019. Changes in Aerosol Chemistry From 2014 to 2016 in Winter in Beijing: Insights From High-Resolution Aerosol Mass Spectrometry. J. Geophys. Res.: Atmos. 124 (2), 1132−1147

Xu, Q., Wang, S., Jiang, J., 2019. Nitrate dominates the chemical composition of PM2.5 during haze event in Beijing, China. Sci. Total. Environ. 689:1293-1303.

Xue, Y., Ho, S. S. H., Huang, Y., Li, B., Wang, L., Dai, W., Cao, J., Lee, S., 2017. Source apportionment of VOCs and their impacts on surface ozone in an industry city of Baoji, Northwestern China. Sci. Rep. 7, 9979, https://doi.org/10.1038/s41598-017-10631-4.

Xue, T., Zheng, Y., Geng, G., Xiao, Q., Meng, X., Wang, M., Li, X., Wu, N., Zhang, Q., Zhu, T., 2020a. Estimating Spatiotemporal Variation in Ambient Ozone Exposure during 2013–2017 Using a Data-Fusion Model. Environ Sci. Technol. 54, 14877-14888.

Xue, Y., Huang, Y., Ho, S.S.H., Chen, L., Wang, L., Lee, S., Cao, J., 2020b. Origin and transformation of ambient

578 volatile organic compounds during a dust-to-haze episode in northwest China. Atmos. Chem. Phys. 20, 5425-
579 5436.
580 Yan, Y., Peng, L., Li, R., Li, Y., Li, L., Bai, H., 2017. Concentration, ozone formation potential and source analysis
581 of volatile organic compounds (VOCs) in a thermal power station centralized area: A study in Shuozhou, China.
582 Environ. Pollut. 223, 295–304.
583 Yang, W.Q., Zhang, Y.L., Wang, X.M., Li, S., Zhu, M., Yu, Q.Q., Li, G.H., Huang, Z.H., Zhang, H.N., Wu, Z.F.,
584 Song, W., Tan, J.H., Shao, M., 2018. Volatile organic compounds at a rural site in Beijing: influence of temporary
585 emission control and wintertime heating. Atmos. Chem. Phys. 18, 12663–12682.
586 Yao, Y.C., Tsai, J.H., Wang, I.T., 2013. Emissionsof gaseous pollutant from motorcycle powered byethanol-
587 gasoline blend. Appl. Energy. 102, 93–100.
588 Yao, Z., Wu, B., Shen, X., Cao, X., Jiang, X., Ye, Y., He, K., 2015. On-road emission characteristics of VOCsfrom
589 rural vehicles and their ozone formation potential in Beijing, China. Atmos. Environ. 105, 91–96.
590 Yao, L., Wang, D., Fu, Q., Qiao, L., Wang, H., Li, L., Sun, W., Li, Q., Wang, L., Yang, X., 2019. The effects of
591 firework regulation on air quality and public health during the Chinese Spring Festival from 2013 to 2017 in a
592 Chinese megacity. Environ Int. 126, 96-106.
593 Yuan, B., Shao, M., Lu, S., Wang, B., 2010. Source profiles of volatile organic compounds associated with solvent
594 use in Beijing, China. Atmos. Environ. 44, 1919–1926.
595 Zhai, S., Jacob, D.J., Wang, X., Shen, L., Li, K., Zhang, Y., Gui, K., Zhao, T., Liao, H., 2019. Fine particulate
596 matter ($PM_{2.5}$) trends in China, 2013–2018: separating contributions from anthropogenic emissions and
597 meteorology, Atmos. Chem. Phys. 19, 11031– 11041, https://doi.org/10.5194/acp-19-11031-2019.

598 Zhang, Y., Wang, X., Zhang, Z., Lu, S., Shao, M., Lee, F.S. C., Yu, J., 2013. Species profiles and normalized re
599 activity of volatile organic compounds from gasoline evaporation in China. Atmos. Environ. 79, 110–118.
600 Zhang, X., Xue, Z., Li, H., Yan, L., Yang, Y., Wang, Y., Duan, J., Li, L., Chai, F., Cheng, M., Zhang, W., 2017.
601 Ambient volatile organic compounds pollution in China. J Environ. Sci. 55, 69-75, 10.1016/j.jes.2016.05.036.
602 Zhang, Y., Li, R., Fu, H., Zhou, D., Chen, J., 2018. Observation and analysis of atmospheric volatile organic
603 compounds in a typical petrochemical area in Yangtze River Delta, China. J. Environ. Sci. 71, 233-248.
604 Zhao, D., Liu, G., Xin, J., Quan, J., Wang, Y., Wang, X., 2020. Haze pollution under a high atmospheric
605 oxidization capacity in summer in Beijing: insights into formation mechanism of atmospheric physicochemical
606 processes. Atmos. Chem. Phys. 20, 4575-4592.
607 Zhao, Q.Y., Bi, J., Liu, Q., Ling, Z.H., Shen, G.F., Chen, F., Qiao, Y.Z., Li, C.Y., Ma, Z.W., 2020. Sources of
608 volatile organic compounds and policy implications for regional ozone pollution control in an urban location of
609 Nanjing, East China. Atmos. Chem. Phys. 20, 3905–3919.
610 Zheng, J., Yu, Y., Mo, Z., Zhang, Z., Wang, X., Yin, S., Peng, K., Yang, Y., Feng, X., Cai, H., 2013. Industrial
611 sector-based volatile organic compound (VOC) source profiles measured in manufacturing facilities in the Pearl
612 River Delta, China. Sci. Total Environ. 456, 127–136.
613 Zheng, H., Kong, S., Xing, X., Mao, Y., Hu, T., Ding, Y., Li, G., Liu, D., Li, S., Qi, S., 2018. Monitoring of
614 volatile organic compounds (VOCs) from an oil and gas station in northwest China for 1 year. Atmos. Chem.
615 Phys. 18, 4567-4595.
616

Figure captions

Figure 1. Time series of meteorological parameters and levels of air pollutants during the sampling period.

Figure 2. Comparison of the concentration and composition of major chemical groups observed in 2019 (this study), 2016 (Liu et al., 2020) and 2014 (Li et al., 2015).

Figure 3. Comparison of major meteorological parameters and air pollutants on clean and polluted days.

Figure 4. Statistic decomposition of meteorological and emission contribution to O_3 and $PM_{2.5}$ levels during different periods.

Figure 5. OFP and SOAFP by chemical groups during different periods.

Figure 6. Ratios of i/n-pentane and toluene/benzene at different $PM_{2.5}$ and O_3 levels. **Figure 7.** Source profiles of VOCs identified using the PMF model and the relative contributions of the individual VOC species.

Figure 8. Contributions of each source to VOCs during different periods.

Figure 9. Contributions of each source to OFP and SOAFP during different periods.

Figure 10. OFP values of the dominant VOC species in the different source categories for the O_3 pollution (a) and compliance (b) days of the O_3-polluted months, and SOAFP values for the $PM_{2.5}$ pollution (c) and compliance (d) days of the $PM_{2.5}$-polluted months.

635

636 **Fig. 1.**

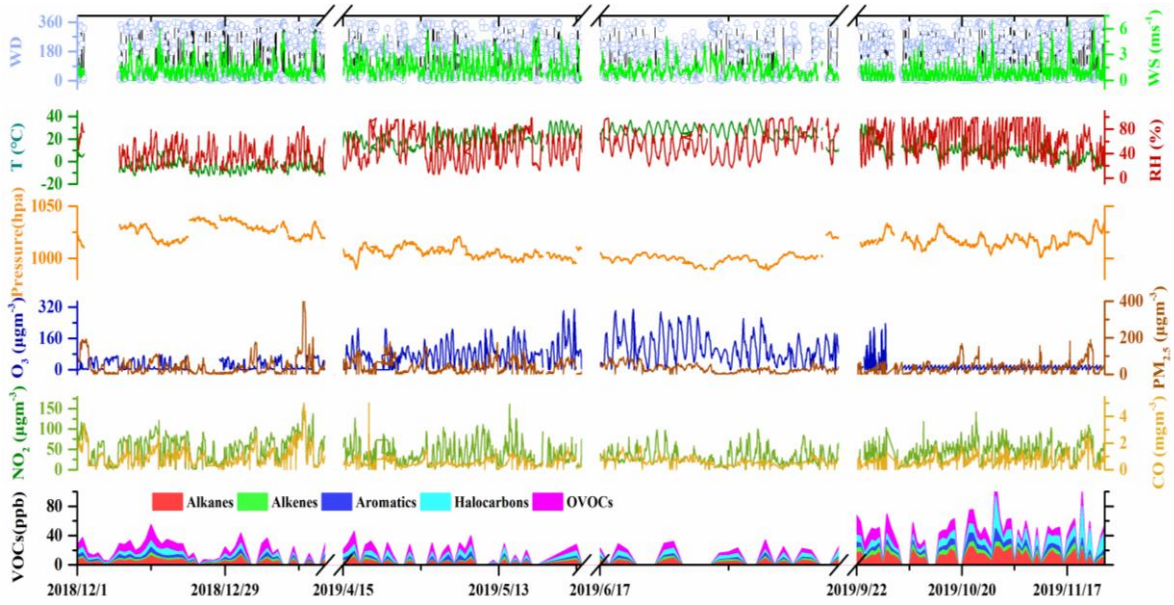

637

Figure 2.

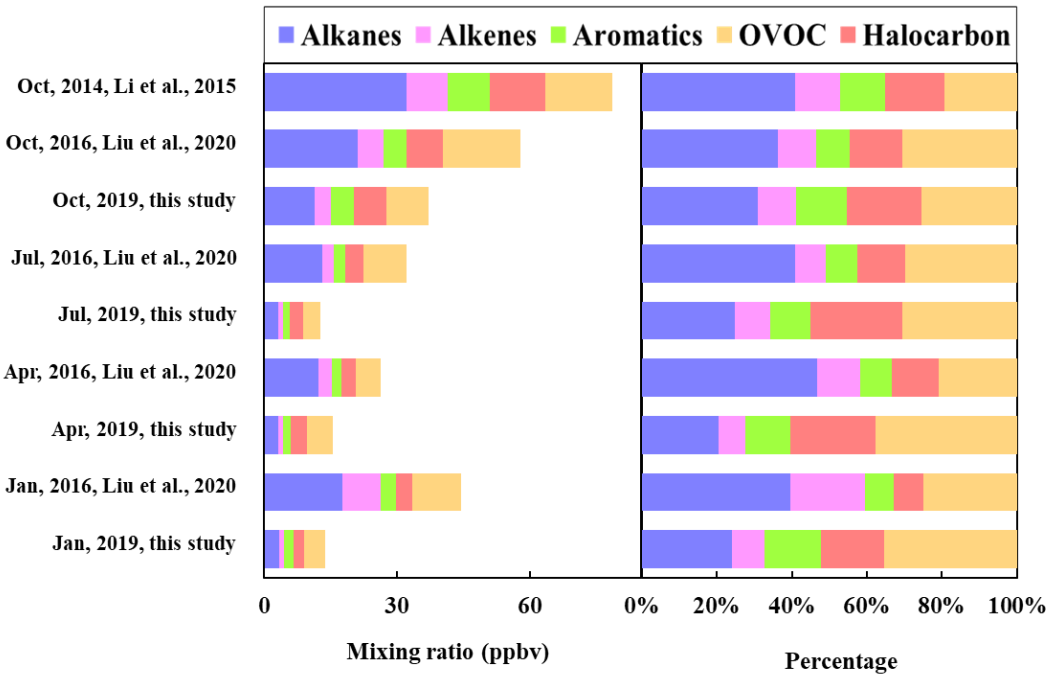
Alkanes
Alkenes
Aromatics
OVOC
Halocarbon
Oct, 2014, Li et al., 2015
Oct, 2016, Liu et al., 2020
Oct, 2019, this study
Jul, 2016, Liu et al., 2020
Jul, 2019, this study
Apr, 2016, Liu et al., 2020
Apr, 2019, this study
Jan, 2016, Liu et al., 2020
Jan, 2019, this study
0
30
60
Mixing ratio (ppbv)
0%
20%
40%
60%
80%
100%
Percentage

Fig. 3.

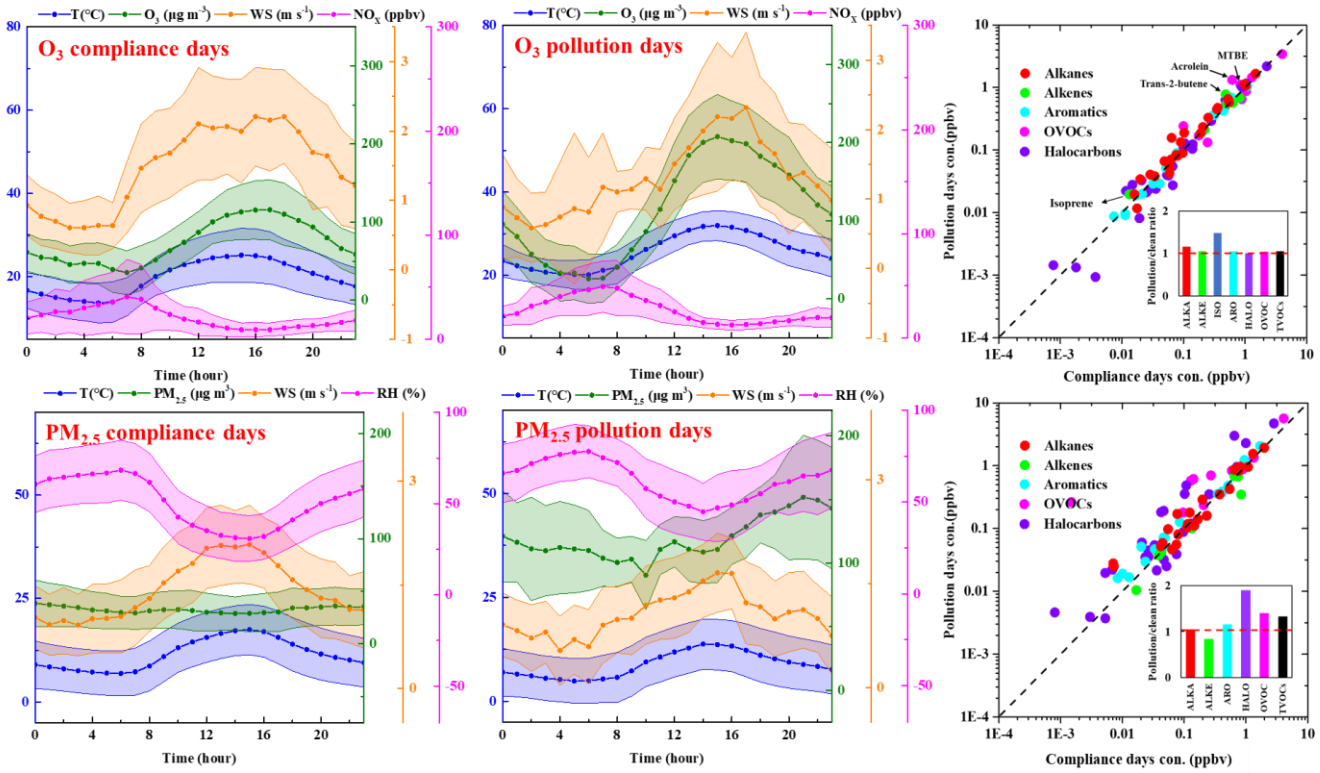
T(°C)
O3 (μg m-3)
WS (m s-1)
NOX (ppbv)
O3 compliance days
O3 pollution days
Time (hour)
PM2.5 (μg m3)
RH (%)
PM2.5 compliance days
PM2.5 pollution days
Alkanes
Alkenes
Aromatics
OVOCs
Halocarbons
MTBE
Acrolein
Trans-2-butene
Isoprene
Pollution days con.(ppbv)
Compliance days con. (ppbv)
Pollution/clean ratio
ALKA
ALKE
ISO
ARO
HALO
OVOC
TVOCs

Fig. 4

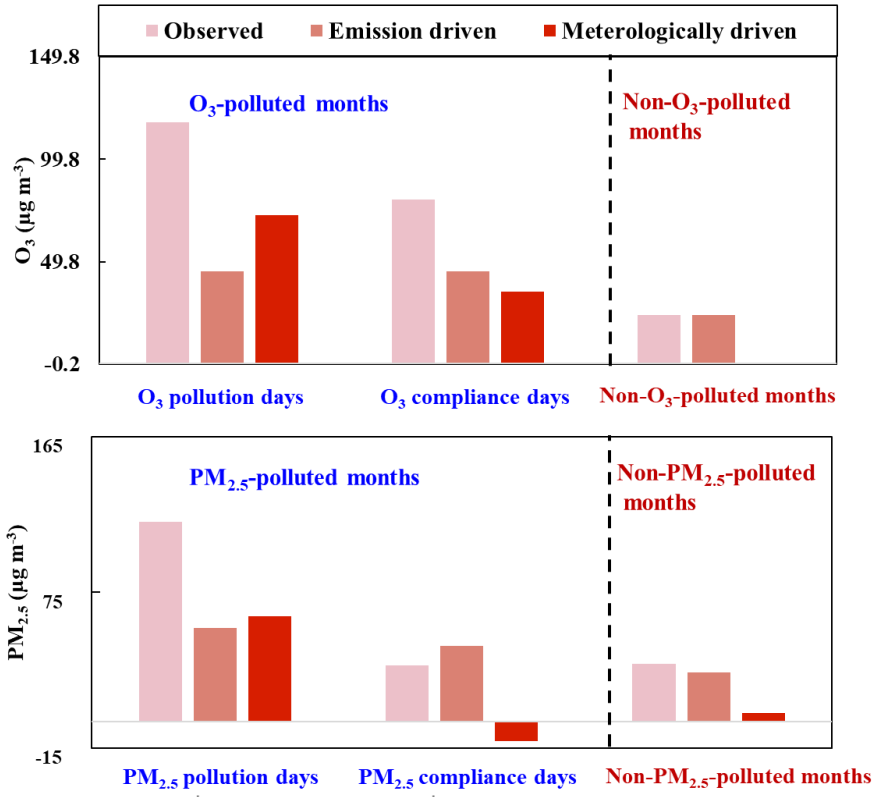
Observed
Emission driven
Meterologically driven
149.8
99.8
49.8
-0.2
O3 (μg m-3)
O3-polluted months
Non-O3-polluted months
O3 pollution days
O3 compliance days
Non-O3-polluted months
165
75
-15
PM2.5 (μg m-3)
PM2.5-polluted months
Non-PM2.5-polluted months
PM2.5 pollution days
PM2.5 compliance days
Non-PM2.5-polluted months

649 **Fig. 5**

650

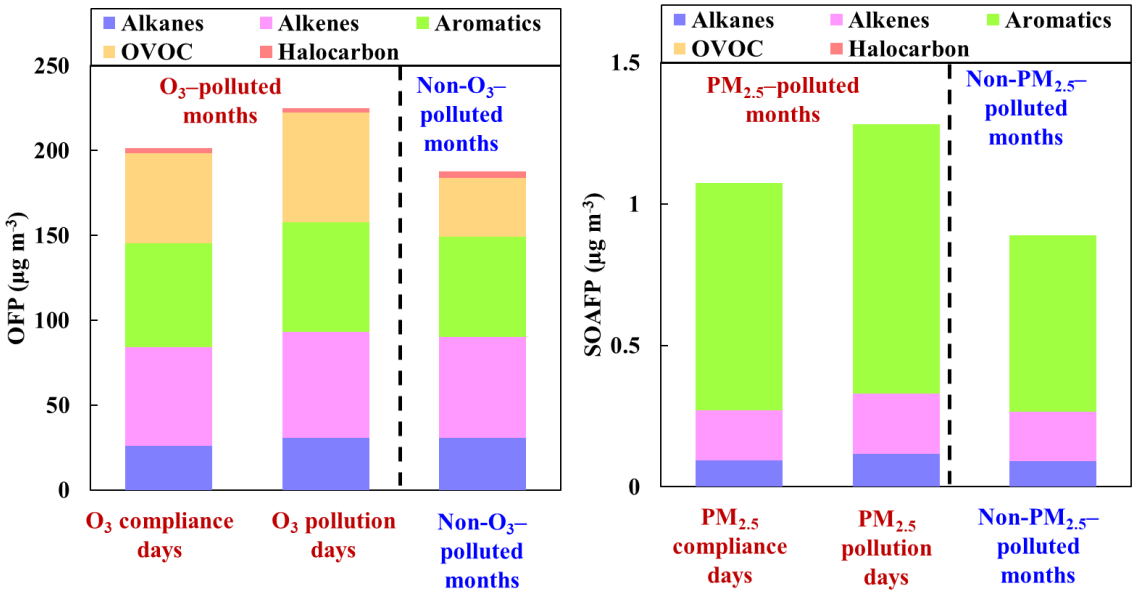

651

Fig. 6

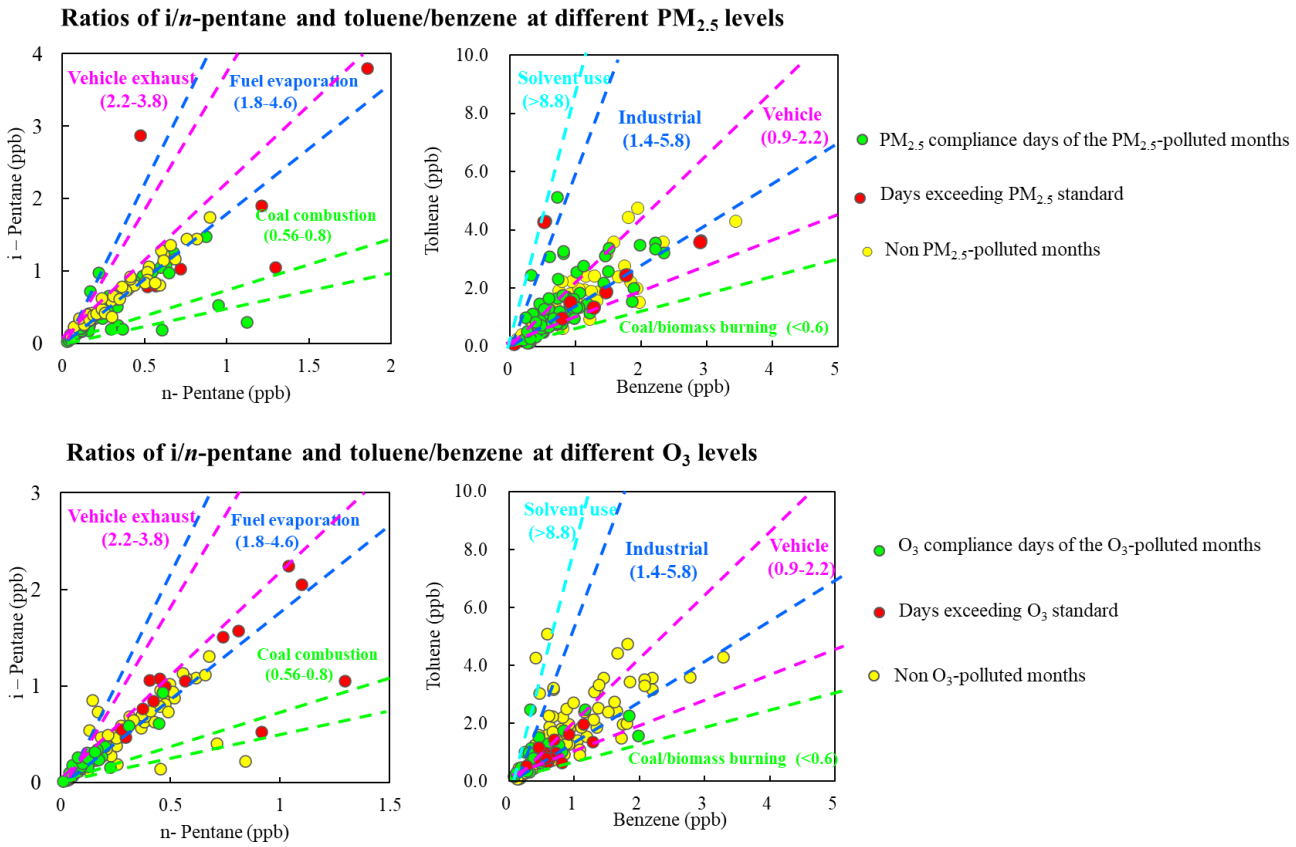
Ratios of i/n-pentane and toluene/benzene at different PM2.5 levels
Vehicle exhaust (2.2-3.8)
Fuel evaporation (1.8-4.6)
Coal combustion (0.56-0.8)
i – Pentane (ppb)
n- Pentane (ppb)
Solvent use (>8.8)
Industrial (1.4-5.8)
Vehicle (0.9-2.2)
Coal/biomass burning (<0.6)
Toluene (ppb)
Benzene (ppb)
PM2.5 compliance days of the PM2.5-polluted months
Days exceeding PM2.5 standard
Non PM2.5-polluted months
Ratios of i/n-pentane and toluene/benzene at different O3 levels
O3 compliance days of the O3-polluted months
Days exceeding O3 standard
Non O3-polluted months

Fig. 7.

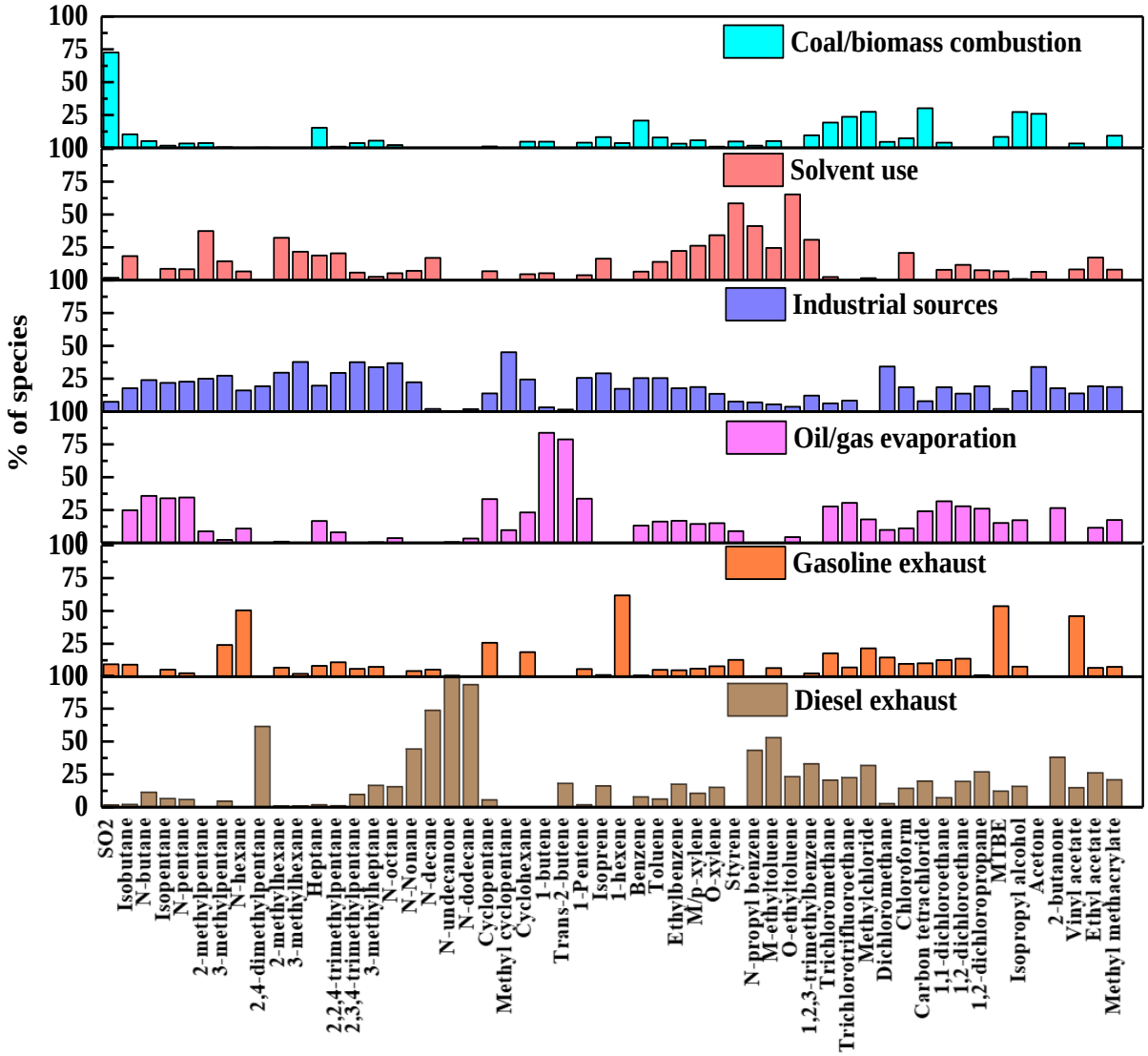
Coal/biomass combustion
Solvent use
Industrial sources
Oil/gas evaporation
Gasoline exhaust
Diesel exhaust
% of species
100
75
50
25
0
SO2
Isobutane
N-butane
Isopentane
N-pentane
2-methylpentane
3-methylpentane
N-hexane
2,4-dimethylpentane
2-methylhexane
3-methylhexane
Heptane
2,2,4-trimethylpentane
2,3,4-trimethylpentane
3-methylheptane
N-octane
N-Nonane
N-decane
N-undecannone
N-dodecane
Cyclopentane
Methyl cyclopentane
Cyclohexane
1-butene
Trans-2-butene
1-Pentene
Isoprene
1-hexene
Benzene
Toluene
Ethylbenzene
M/p-xylene
O-xylene
Styrene
N-propyl benzene
M-ethyltoluene
O-ethyltoluene
1,2,3-trimethylbenzene
Trichloromethane
Trichlorotrifluoroethane
Methylchloride
Dichloromethane
Chloroform
Carbon tetrachloride
1,1-dichloroethane
1,2-dichloroethane
1,2-dichloropropane
MTBE
Isopropyl alcohol
Acetone
2-butanone
Vinyl acetate
Ethyl acetate
Methyl methacrylate

Fig. 8

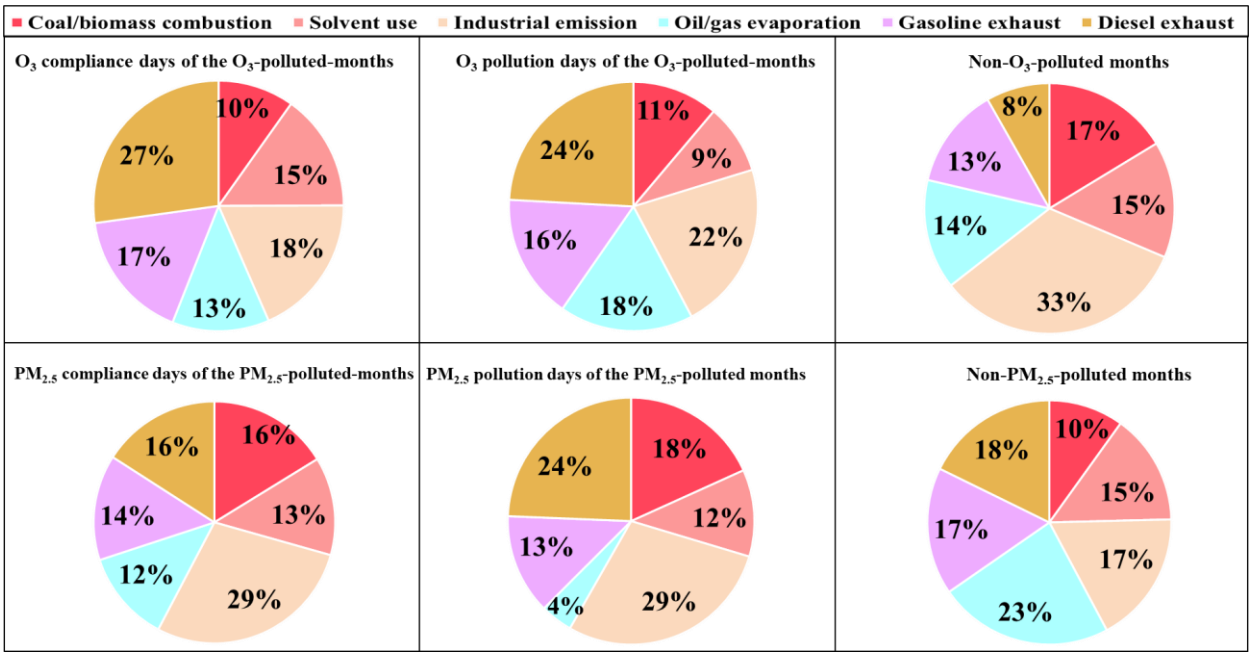
Coal/biomass combustion
Solvent use
Industrial emission
Oil/gas evaporation
Gasoline exhaust
Diesel exhaust
O3 compliance days of the O3-polluted-months
10%
15%
18%
13%
17%
27%
O3 pollution days of the O3-polluted-months
11%
9%
22%
18%
16%
24%
Non-O3-polluted months
17%
15%
33%
14%
13%
8%
PM2.5 compliance days of the PM2.5-polluted-months
16%
13%
29%
12%
14%
16%
PM2.5 pollution days of the PM2.5-polluted months
18%
12%
29%
4%
13%
24%
Non-PM2.5-polluted months
10%
15%
17%
23%
17%
18%

Fig. 9

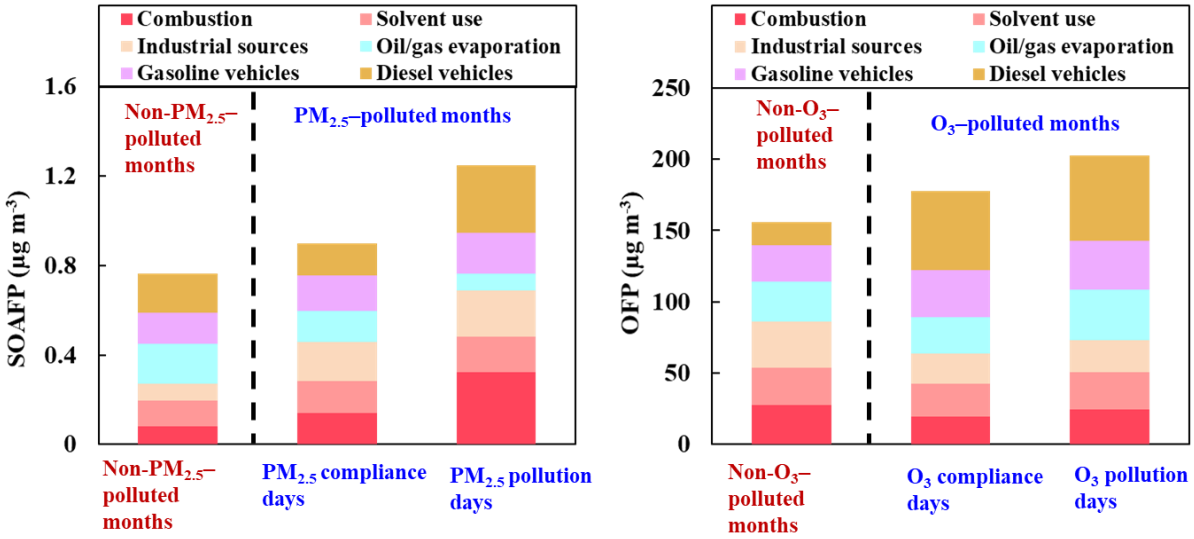
Combustion
Solvent use
Industrial sources
Oil/gas evaporation
Gasoline vehicles
Diesel vehicles
SOAFP (μg m-3)
1.6
1.2
0.8
0.4
0
Non-PM2.5–polluted months
PM2.5–polluted months
Non-PM2.5–polluted months
PM2.5 compliance days
PM2.5 pollution days
OFP (μg m-3)
250
200
150
100
50
0
Non-O3–polluted months
O3–polluted months
Non-O3–polluted months
O3 compliance days
O3 pollution days

667 **Fig. 10**

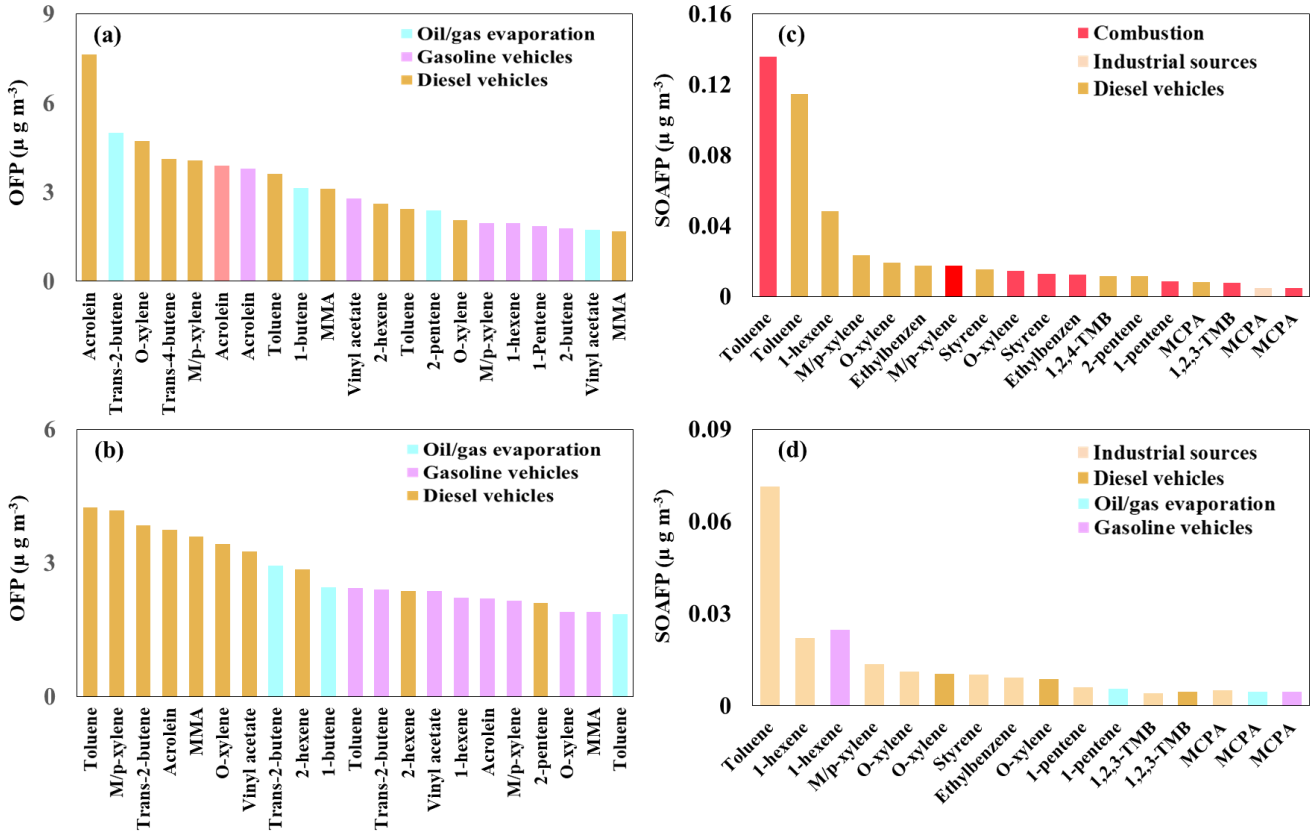

668